Hypertrophic cardiomyopathy-linked variants of cardiac myosin binding protein C3 display altered molecular properties and actin interaction

Sahar I. DAAS‡†, Khalid FAKHRO‡†#, Angelos THANASSOULAS§, Navaneethakrishnan KRISHNAMOORTHY‡^, Alaaeldin SALEH*, Brian L. CALVER[ƨ], Bared SAFIEH-GARABEDIAN*, Egon TOFT*, George NOUNESIS§, F. Anthony LAI*[ƨ°] and Michail NOMIKOS*[1]

‡Translational Medicine, Sidra Medicine, Doha, Qatar

†College of Health and Life Sciences, Hamad Bin Khalifa University, Doha, Qatar

#Weill Cornell Medical College, Doha, Qatar

§National Center for Scientific Research "Demokritos", Aghia Paraskevi, Greece

^Heart Science Centre, National Heart & Lung Institute, Imperial College London, UK

*College of Medicine, Member of QU Health, Qatar University, Doha, Qatar

ƨCollege of Biomedical & Life Sciences, Cardiff University, UK

°Biomedical Research Center, Qatar University Doha, Qatar

[1]Correspondence to:

Michail Nomikos: mixosn@yahoo.com or mnomikos@qu.edu.qa

College of Medicine, Member of QU Health

Qatar University

Doha, PO BOX: 2713, Qatar

Phone: +974 44037846

Abbreviations: HCM, hypertrophic cardiomyopathy; *c-MYBPC3*, cardiac myosin binding protein C3; CD, circular dichroism; GuHCl, guanidine hydrochloride

ABSTRACT

The most common inherited cardiac disorder, hypertrophic cardiomyopathy (HCM), is characterized by thickening of heart muscle, for which genetic mutations in cardiac myosin-binding protein C3 (*c-MYBPC3*) gene, is the leading cause. Notably, patients with HCM display a heterogeneous clinical presentation, onset and prognosis. Thus, delineating the molecular mechanisms that explain how disparate *c-MYBPC3* variants lead to HCM is essential for correlating the impact of specific genotypes on clinical severity. Herein, five *c-MYBPC3* missense variants clinically associated with HCM were investigated; namely V1 (R177H), V2 (A216T), V3 (E258K), V4 (E441K) and double mutation V5 (V3+V4), all located within the C1 & C2 domains of MyBP-C, a region known to interact with sarcomeric protein, actin. Injection of the variant complementary RNAs in zebrafish embryos were observed to recapitulate phenotypic aspects of HCM in patients. Interestingly, V3- and V5-cRNA injection produced the most severe zebrafish cardiac phenotype, exhibiting increased diastolic/systolic myocardial thickness and significantly reduced heart rate compared to control zebrafish. Molecular analysis of recombinant C0-C2 protein fragments revealed that *c-MYBPC3* variants alter the C0-C2 domain secondary structure, thermodynamic stability and importantly, result in a reduced binding affinity to cardiac actin. V5 (double mutant), displayed the greatest protein instability with concomitant loss of actin binding function. Our study provides specific mechanistic insight into how *c-MYBPC3* pathogenic variants alter both functional and structural characteristics of C0-C2 domains leading to impaired actin interaction and reduced contractility, which may provide a basis for elucidating the disease mechanism in HCM patients with *c-MYBPC3* mutations.

Keywords:

Hypertrophic cardiomyopathy, Cardiac myosin binding protein C3, *c-MYBPC3* mutations, Zebrafish, Actin

Introduction

Hypertrophic cardiomyopathy (HCM) is a common inherited heart disease with an estimated prevalence of 2-5 per 1000 [1, 2] that is characterized by cardiac impairment linked to increased left ventricular wall thickness, diastolic dysfunction, interstitial fibrosis and myocyte disarray [3, 4]. Clinical presentation of HCM patients is heterogeneous, ranging from asymptomatic or mildly symptomatic, to distinct features such as dyspnea, angina, syncope, leading in some cases to progressive heart failure [1, 5, 6]. HCM is a genetic autosomal dominant disease characterized by extensive allelic heterogeneity affecting both sarcomeric and sarcomere-related proteins. Variants of the cardiac myosin binding protein C3 (*c-MYBPC3*) gene encoding the sarcomeric protein MyBP-C are the most common genetic cause of HCM, representing 40–50% of all HCM mutations [1, 7, 8]. Variants with different pathogenicity classification are associated with heterogeneous HCM clinical presentation, disease onset and prognosis [9-13]. Thus, analysis of structural-functional correlations is necessary to understand the molecular mechanisms by which these variants lead to HCM. It has been hypothesized that *c-MYBPC3* missense mutations directly disrupt the topology of MyBP-C by causing protein misfolding that impairs protein function [14]. The N-terminal domains of MyBP-C - C0, C1 motif and C2 were previously found to play significant roles in regulating cardiac muscle contraction via their interaction with myosin [15] and actin [16], while its C-terminus was recently reported to directly interact with cardiac ryanodine receptor type 2 (RyR2) [17]. Considering the spectrum of HCM phenotypes described, we hypothesized that missense variation may disparately impact the structure of the protein and differentially affect its functional interactions [11, 18-20]; hence, in this study we selected five *c-MYBPC3* variants linked with HCM for structural and functional characterization. Three variants (V1-3) (V1,

Arg177His; V2, Ala216Thr; V3, Glu258Lys) all located within the C1 domain, and V4 (Glu441Lys) within C2 domain were identified in an Egyptian HCM study [21], while V5 is a double mutant (V3 & V4) that has been associated with a severe, early-onset HCM phenotype [11]. We hypothesized that these variants affect the biophysical and biochemical characteristics of MyBP-C, altering the functional properties of the C1 and C2 domains specifically leading to altered MyBP-C-actin association within the sarcomere. To characterize the *in vivo* effects of these variants, we employed a zebrafish model to elucidate morphometric consequences on cardiac function after synthetic mRNA injections. We also generated the mutant and wild-type N-terminal MyBP-C C0-C2 domains as recombinant proteins to examine their biophysical and biochemical properties, as well as their *in vitro* interaction with cardiac actin. Injection of zebrafish embryos with synthetic mRNA corresponding to the five MyBP-C variants produced atypical cardiac morphology and impaired cardiac function recapitulating the human HCM phenotype. Collectively, our results provide insight into the molecular impact of variant-specific *c-MYBPC3* genotype on MyBP-C biophysical characteristics, protein stability and functional interaction with cardiac actin, contributing to a better understanding of HCM genotype-clinical severity correlation.

Experimental

Materials and methods

Classification of identified variants

We used the ClinVar database (https://www.ncbi.nlm.nih.gov/clinvar/) for *c-MYBPC3* variant selection with variable pathogenicity classification as: pathogenic, nonpathogenic, or as a variant of unknown clinical significance (unlikely to be pathogenic, uncertain, likely to be pathogenic).

Zebrafish model

All procedures were performed in conformity with the AAALAC International, Guidance on the housing and care of Zebrafish (Danio rerio) [22]. The study protocol was approved by Qatar University IACUC Office under project approval number QU-IACUC 015/2014. Zebrafish were raised and maintained at 28°C on a 14:10-h light-dark cycle and fed *Artemia nauplii*. Wild-type (AB) strain of zebrafish was used for our experiments.

Human *c-MYBPC3* missense mutation in vitro transcription of mRNA

Wild-type (WT) *c-MYBPC3* cDNA (NM_001044349) and the five mutant constructs were cloned into pcDNA-DEST47 vector (Life Technologies) to generate human WT *c-MYBPC3* mRNA and mRNA encoding the four single missense variants : V1 (c.530G>A), V2 (c.646G>A), V3 (c.772G>A), V4 (c.1321G>A) as well as the double variant V5 (c.772G>A + c.1321G>A) (Figure 1). RNA transcription was performed using the mMESSAGE mMACHINE T7 Transcription Kit, Cat # AM1344 and Poly(A) Tailing Kit, Cat # AM1350 (ThermoFisher Scientific).

Morpholino design and synthetic mRNA injection

The *c-mybpc3* morpholino (MO:5'-CTCTGGCATCCTGGTTGAGTGTCCC-3', Gene Tools, USA) targeted against the translational start site was injected into WT strain zebrafish embryos at one cell stage to knock down zebrafish endogenous *c-mybpc3* [23]. In the mRNA experiments, *c-mybpc3* MO (2.5 ng) was co-injected with human *c-MYBPC3* mRNA (100 pg) for the corresponding missense *c-MYBPC3* variants. At least 50 embryos were injected in each group.

Quantitative measurements of zebrafish cardiac size and function

Injected zebrafish embryos were raised at 28°C for 3 days and individually removed from the 28°C incubator immediately prior to measurement to minimize the effect of environmental temperature on cardiac function. Zebrafish embryos were mounted in 3% methylcellulose prior to imaging. The cardiac phenotypes were recorded at 60 frames/second for 3 seconds at 150 X using a stereomicroscope (SteREO Zeiss LUMAR.V12) equipped with USB 2.0 monochrome camera (The Imaging Source).

Measurement of zebrafish ventricular myocardial thickness

Structural analysis of the zebrafish ventricle was performed by analysis of 2D images at specific time points. Recorded videos were imported into Image J software (version 1.45s public domain software, http://imagej.nih.gov/ij) and ventricular end-diastole and ventricular end-systole images were extracted. The endocardial and myocardial boundaries were traced to calculate the ventricular wall thickness as the average thickness between these two regions.

Heart Rate Measurements

Recorded videos were imported into DanioScope software (Noldus, version 1.0.109) as a compressed AVI file, where a subset of the beating heart was outlined and heart rate was calculated.

Statistical analysis

Statistical analysis was performed using GraphPad Prism 7. Multiple group comparisons were analyzed by one-way ANOVA. Significant difference between groups was expressed using p values: *$p<0.05$, **$p<0.01$, ***$p<0.001$, ****$p<0.0001$.

Molecular Modeling

The complex MyBP-C structure of C1-C2 domains was obtained from our previous molecular dynamics study of 10ns simulations at physiological conditions, with all the parameters as described earlier [11]. The representative structures of WT MyBP-C and its variants from the molecular dynamics simulations were selected using cluster analysis. In this, 1000 structures of each variant trajectory were classified into clusters based on their structural deviations. A structure from the top ranked cluster was chosen for representation, as it was a frequently occurring conformation. These simulated structures utilized PyMol (www.pymol.org) for analysis of the secondary structural elements. To quantify the structural components, we used a secondary structure assignment program in PyMOL ("STRIDE") to calculate all the elements. In addition, to map the structural deviations of variants from the WT, we used molecular superposition of the representative structures by aligning using the graphical interface in

PyMOL. All protein cartoons were generated with high ray trace mode with depth cue to give 3D representation of the molecular models.

Plasmid construction

Human *c-MYBPC3* cDNA (NM_001044349) was amplified by PCR from pcDNA-DEST47, using Phusion polymerase (Finnzymes) and the appropriate primers to incorporate 5'-EcoRI and 3'-NotI sites. *c-MYBPC3* was then cloned into pHSIE vector. The primers used for the amplification of *c-MYBPC3* were: 5'-GGAAGGTACCATGGCTGATCAGCTGACCGAAG-3' (forward) and 5'-GCAAGCGGCCGCTCATTTTGCAGTCATCATCTGTAC-3' (reverse).

Prokaryotic expression, purification and intein cleavage of MyBP-C C0-C2 domain recombinant proteins

For MyBP-C-fusion protein expression (6xHis-SUMO2-intein-C0-C2), *Escherichia coli* [BL21-CodonPlus(DE3)-RILP; Stratagene] were transformed with the appropriate plasmid. The presence of the SUMO fusion-tag facilitated enhanced solubility of the recombinant protein in bacterial cells [24, 25]. Cells were cultured at 37 °C until the optical density at 600 nm reached 0.6. Fusion protein expression was then induced for 18 h at 16°C with 0.1 mM IPTG (isopropyl *β*-D-thiogalactopyranoside). Bacterial cell pellets were harvested by centrifugation at 6,000 g for 15 minutes, 4°C and then resuspended in 20 ml of buffer A (50 mM Tris, pH 8.5, 300 mM NaCl, 25 mM imidazole). Cells were lysed by mild sonication then partitioned into soluble and insoluble fractions by centrifugation at 20,000 g for 20 minutes at 4°C and the supernatant containing the soluble protein fraction was transferred into a fresh tube. Supernatant was then

applied to a 1ml Ni–NTA column pre-equilibrated in buffer A. To avoid auto-cleavage by intein protease, all the following purification steps were performed at 4°C using ice-cold buffers. After binding, the column was washed with 10 x column volumes of buffer A followed by an additional wash (10 x column volumes) of cleaving buffer (PBS buffer supplemented with 40 mM Bis-Tris and 25 mM imidazole, pH 6.0). After the second wash, the column was sealed and incubated at room temperature for 3 h to allow intein cleavage. After intein cleavage, 5 ml of cleaving buffer was used to elute the cleaved C0-C2 (MyBP-C) proteins from the resin. The remaining proteins bound to the column were eluted with 10 ml of cleaving buffer supplemented with 500 mM imidazole, and the eluted fractions were collected and analysed by 12% SDS–PAGE electrophoresis.

Western Blotting

Purified recombinant MyBP-C C0-C2 proteins were analyzed by SDS-PAGE electrophoresis with Coomassie Brilliant Blue staining and immunoblot analysis performed as described previously [26]. Proteins were probed with a polyclonal anti-MyBP-C antibody (1:1,000 dilution) (Abgent, Cat # AP12436a) and immunoreactive proteins were detected by ECL Chemiluminescence Detection Kit (Thermofisher Scientific, Cat #32106).

Circular Dichroism (CD) Analysis

CD measurements were conducted using a JASCO-715 spectropolarimeter with a Peltier type cell holder. Wavelength scans in the 190 nm to 260 nm range (far-UV region) were performed in Quartz SUPRASIL (HELLMA) precision cells of 0.1 cm path length, using a wavelength step of 0.2 nm, a scan rate of 20 nm min^{-1}, response time 1 s and 1 nm bandwidth.

Buffer spectra were collected and subtracted from all scans. The concentration of all protein samples was 0.2 mg/ml.

Thermal denaturation data were collected by heating the protein sample from 20° to 90°C using a scan rate of 1.5 K/min and monitoring signal changes at 208 nm. Spectral parameters for these measurements were: 1 s step resolution, 0.5 s response time, sensitivity 25 mdeg and bandwidth 1 nm. Data analysis software (CDNN version 2.1) was used to deconvolute the collected far-UV CD spectra in order to determine the protein's α-helix, anti and parallel β-sheet, β-turn and random coil content.

Chemical Denaturation

Fluorescence spectra were collected on a PTI QuantaMaster 400 steady-state fluorescence system. Tryptophan was selectively excited at 295 nm and emission spectra were collected between 310 to 450 nm using a 4 ml quartz cuvette (Hellma) with a path length of 10 mm. Scan rate was set to 100 nm min^{-1} with a response time of 1 sec. Slit width for both emission and excitation were 2 nm. The protein species concentration used for all fluorescence experiments was 0.2 mg/ml. All fluorescence spectra were corrected for background intensity as measured with pure buffer. In a typical experiment, small amounts of an 8 M guanidine hydrochloride solution were gradually added in the cuvette along with the appropriate amount of concentrated protein solution in order to keep the MyBP-C concentration in the cell constant. The mixture was stirred using a small magnetic stir bar for 1 min and incubated in the dark for 15 min, at which point the fluorescence emission spectrum of the sample was collected. The titration was carried on until a 5 M final concentration of guanidine hydrochloride was reached

inside the cuvette. Mock titrations with the addition of buffer instead of guanidine hydrochloride were collected and the corresponding spectra were subtracted from the original data.

The final data were fitted using the following equation [27]:

$$F = \frac{(a_N + b_N \cdot [D]) + (a_D + b_D \cdot [D]) \cdot e^{-(\frac{\Delta G}{RT})}}{1 + e^{-(\frac{\Delta G}{RT})}}$$

where: $\Delta G = m([D^{50\%}] - [D])$, [D] is the concentration of the denaturant in the cuvette, $[D^{50\%}]$ is the concentration of denaturant at the midpoint of the transition, m is the slope of the denaturation transition, R is the universal gas constant, T is the experimental temperature, a_N and b_N the intercept and slope of the native state baseline, while a_D and b_D are the corresponding values of the denatured state baseline.

Co-sedimentation Cardiac Actin Binding Assays

Co-sedimentation assays were performed as previously described [28]. Actin Binding Protein Biochem Kit (Cytoskeleton, Cat # BK001) and bovine cardiac actin (Cytoskeleton, Cat # AD99-B) were used. Bovine cardiac actin was prepared in General Actin Buffer (5 mM Tris-HCl pH 8.0, 0.2 mM CaCl2) (Cytoskeleton, Cat # BSA01) and supplemented with 0.2 mM ATP and 0.5 mM DTT prior to use. Purified N-terminal C0-C2 MyBP-C protein fragments were dialyzed using Vivaspin tubes (Sartorius, Vivaspin 20). Initially, optimization experiments were performed using 2 μM of wild type MyBP-C C0-C2 and 1, 10, 20 or 30 μM c-actin, in order to identify the optimal concentration in which saturated binding between MyBP-C and c-actin is achieved. After the optimal concentrations were determined, 30 μM of c-actin was incubated with 2 μM of each MyBP-C C0-C2 recombinant protein (wild-type and mutants) for 30 min at room temperature. For our co-sedimentation experiments, incubation of c-actin with α-actinin

protein served as our positive control, while incubation of c-actin with BSA served as our negative control. After incubation, samples were centrifuged at 14,000 g for 1 hour at 24 °C. Supernatants were carefully removed, mixed with 10 µl of 5 x Laemmli reducing-sample buffer and analyzed by SDS-PAGE electrophoresis and Coomassie brilliant blue staining. Finally, to estimate the relative binding of c-actin to the various recombinant proteins, band intensities appearing in the stained gels were measured by densitometric analysis and the data analyzed using GraphPad Prism 7.

Results

c-MYBPC3 variants are associated with distinct HCM phenotype

The elucidation of genotype-phenotype associations provides a crucial parameter to help predict the impact of a specific variant on HCM clinical severity. To investigate the mechanism by which different *c-MYBPC3* variants lead to cardiac impairment, we studied four single missense mutations: V1 (c.530G>A, p.R177H), V2 (c.646G>A, p.A216T), V3 (c.772G>A, p.E258K), V4 (c.1321G>A, p.E441K) in addition to a double mutation V5 (V3+V4), (Figure 1). HCM patients expressing these variants exhibited a range of clinical symptoms and variable degrees of ventricular hypertrophy as determined by septum and wall thickness (Table 1). Multiple *in silico* algorithms, and/or population frequency databases defined the five variants' pathogenicity classification that varied from uncertain significance to certainly pathogenic. Furthermore, the patient carrying the double mutation (V5) had an early-onset disease at age 21 and died at the age of 42. Conversely, patients carrying single mutations (V1, V2, V3, and V4) had lower severity symptoms leading to heart failure later on in life (Table 1) suggesting that

patients expressing different *c-MYBPC3* variants can present with typical HCM clinical heterogeneity in regard to disease severity, onset and prognosis.

Modeling HCM patients' *c-MYBPC3* variants using zebrafish

Zebrafish (*Danio rerio*) is a powerful vertebrate animal model to study cardiac function due to its embryonic transparency [29]. To assess variants' genotype-phenotype associations, we injected synthetic mRNA encoding *c-MYBPC3* variants at the zebrafish one-cell stage and examined their cardiac morphology and function. The injection of synthetic mRNA resulted in aberrant cardiac morphology with altered ventricular sizes and function when examined at 3 days post-fertilization (dpf) (Figure 2, supplemental video 1). V1, V2 and V4 displayed notably different ventricular morphology to the control group. However, V5 and V3 exhibited a greater disparity in ventricular phenotype compared to other variants (Figure 2B, supplemental video 1). These results demonstrate that *c-MYBPC3* V5 and V3 zebrafish cardiac phenotypes correlate with their pathogenicity classification in HCM patients, as both are predicted to be pathogenic class 5 (Table 1). Thus, expression of these variants in the zebrafish model essentially recapitulated the HCM pathological cardiac phenotype in comparison to controls (Figure 2A-B).

Zebrafish *c-MYBPC3* models develop increased ventricular myocardial thickness

Cardiac morphometric measurement of the ventricular myocardial wall thickness of *c-MYBPC3* variant-injected embryos was determined at both diastole and systole (Figure 2C-D). All *c-MYBPC3* variants resulted in a significantly increased ventricular myocardial thicknesses

in comparison to control group. The V5 (V3 & V4) double mutation, and V3 (E258K) exhibited the most severe myocardial hypertrophic phenotype with increased diastolic / systolic myocardial thickness at 15.6 / 14.6 μm ($p<0.0001$) and 14.2 / 12.9 μm ($p<0.0001$), respectively. While thickness for V1 (R177H) was 12.7 / 12.5 μm ($p<0.0001$), V2 (A216T) yielded 11.5 / 11.7 μm ($p<0.001$) and V4 (E441K) displayed 12.1 / 12.3 μm ($p<0.0001$) in contrast to control zebrafish at 10.1 / 9.5 μm (Figure 2C-D). Zebrafish cardiac phenotype resembled the human ventricular hypertrophic phenotype as HCM patients exhibit increased myocardial wall thickness with a heterogeneous clinical presentation among patients [30].

Zebrafish *c-MYBPC3* models develop impaired cardiac contractility

To examine whether the *c-MYBPC3* variants elicit different effects on cardiac function, we assessed the heart rate of injected zebrafish as an indicator of cardiac contractile impairment. Introduction of both V3 and V5 synthetic mRNA significantly affected the average heart rate resulting in a 23% reduction for both groups; 113 beats per minute (bpm) compared to the level observed in zebrafish controls at 146 bpm. In contrast, there was a moderate decrease (<10%) for V1, V2, and V4, at 138, 143 and 133 bpm, respectively; however, these still represent cardiac contractile impairment (Figure 2E). These findings suggest that genotype specificity contributes to HCM phenotypic severity as the V5 double mutation produces early-onset and progression to end-stage HCM (Table 1). Indeed, mRNA injection corresponding to V5 variant in zebrafish resulted in the most severe heart rhythm impairment (Figure 2B-E).

Bioinformatics analysis of *c-MYBPC3* variant effect on functional domains

The severe phenotypes of V3 and V5 led us to study structure-function relationships at protein level, which may reveal molecular determinants that underlie genotype to phenotypic expressions. Several studies have reported that the region C1-C2 of MyBP-C plays a central role in the interactions with actin and myosin proteins within the sarcomere [31, 32]. Our molecular model of the C1-C2 region of the WT protein suggests this linker segment (MyBP-C motif) may hold the key sites for protein phosphorylation (Figure 3A). The secondary structural elements of the domains C1 and C2 in the WT comprises β-sheets, however, the linker/motif is highly α-helical in nature. Both the V3 and V5 molecular models deviated structurally and were arranged differently from WT, with the majority of these rearrangements observed in the motif region (Figure 3B-C). The variants induced changes in the secondary structural elements of the C1 and C2 domains and in the intervening motif region, where the impact was in particular, higher in V5 (Figure 3C) in comparison to V3. Interestingly, V3 appeared to be flexible, while V5 appeared to be rigid compared to WT in the RMSD (root mean square deviation) calculation of the representative structures from molecular dynamics simulations (Figure 3D). The secondary structural changes shown in the graph (Figure 3E) provides an overview of the intra-molecular consequences that induce structural rearrangements in both V5 and V3. Here, the V3 model presents reduced β-sheets and increased coils compared to WT, whereas V5 showed inverse behavior. This correlates with our deviation analysis and reflects V3 flexibility with increase of coils, and the rigid V5 upon reduction of coils with increased β-sheets. Overall, this protein modeling helps to provide a molecular insight into the structural consequences of MyBP-C variants.

Circular dichroism (CD) spectroscopy and thermal stability analysis of MyBP-C variants

To investigate the impact of these *c-MYBPC3* variants on the biophysical and biochemical properties of WT MyBP-C protein, we generated prokaryotic expression plasmid constructs encoding the C0-C2 N-terminal domains of WT and the five variants (Figure 4A). The purified recombinant C0-C2 fragment proteins were highly soluble and migrated on SDS-PAGE according to their predicted molecular weight of ~50 kDa, as shown in both Coomassie stained gel and western blot analysis using MyBP-C N-terminal antibody (Figure 4B**).** To better understand the structural effects of these *c-MYBPC3* variants, we measured far-UV CD spectra (Figure 4C) and we determined the secondary structure elements (Table 2) of all protein samples at 25°C. It was evident that all variants disrupted the native structure of the C0-C2 proteins, leading to conformations with significantly different secondary structure characteristics when compared to WT (Table 2). At elevated temperatures (~90°C), all protein species retain most of their secondary structure characteristics (Supplemental material, Tables 1-6). However, for WT, V1 and V2, we observed an increase in random coil content with a concurrent loss of helicity, reflecting partial unfolding of the structure. At the same time, the β-sheet content of the protein fragments remained relatively intact, revealing a central core of β-sheets with high thermal stability. For V3, V4 and V5 only small changes in the secondary structure content were observed. This was also evident from the relatively small molar ellipticity change recorded in the far-UV spectra throughout the 20°C - 90°C temperature range. Most likely, the observed changes involved spatial rearrangement of the secondary structure elements without significant unfolding. CD melting curves were collected to analyze the thermal denaturation profiles at 208 nm over the temperature range 20°C - 90°C (Figure 5). The relative signal change for V3, V4 and V5 was small, resulting in curves with lower signal to noise ratio than the corresponding profiles of WT, V1, and V2. The thermal denaturation curve of WT, V1, V2, V3 and V4 revealed the presence of

two consecutive unfolding transitions; the first thermal transition occurs in the temperature range 50°C - 65°C with the second at 65°C - 90°C. Interestingly, in contrast to other variants, the melting profile of V5 exhibits only the unfolding transition at 50°C - 65°C, suggesting that no further protein aggregation occurred after ~60°C for this fragment. A possible mechanism for this complex thermal behavior involves the formation of oligomers from monomer protein fragments (first transition). As the temperature of the sample increases, partial unfolding and structural rearrangements of the proteins, dictated by further changes in their aggregation state, result in a second thermal transition. A similar thermal behavior has been previously reported for other MyBP-C motifs [33, 34] with dynamic light scattering studies confirming the formation of aggregates upon heating [34].

Chemical denaturation profiles for the WT and mutant MyBP-C proteins

To determine the thermodynamic stability of mutant MyBP-C protein fragments, we tested the reversibility of chemically-induced transitions to calculate the Gibbs free energy change (ΔG) of the unfolding process (Table 3). Chemical denaturation profiles of WT and MyBP-C recombinant fragment proteins exhibited transitions that were completely reversible and under thermodynamic control, with all samples recovering their initial spectra after dialysis into their original buffer (Figure 6). Interestingly, except for V5, chemical denaturation of all variants lead to conformations with increased stability compared to the WT MyBP-C fragment. Notably, V3 and V4 showed a significant increase in ΔG (~1.5 kcal/mol), while for V1 and V2 this change was less than 0.6 kcal/mol, slightly above the statistical error for these measurements. The recorded V5 destabilizing effect is small and lower than the corresponding statistical error, indicating that V5 has practically no impact on the thermodynamic stability of

MyBP-C. Thermodynamic analysis for the chemical-induced denaturation of all fragments (Table 3) showed ΔG values lower than the typical 5-15 kcal/mol found for most proteins [27].

MyBP-C variants affect cardiac function through impaired actin binding

MyBP-C is a multi-domain protein with vital structural and regulatory roles. The selected variants are located within the N-terminal region, which encompasses the C1-C2 domains of MyBP-C that is involved in regulating cardiac muscle contraction through interaction with actin within the sarcomere (Figure 4A). The recombinant C0-C2 domains have been previously shown to interact with actin [16]. Thus, we hypothesized that impaired cardiac function phenotypes may be correlated with a reduced ability of MyBP-C to interact with actin. To investigate the specific effects of the variant's structural alterations on actin binding properties, we employed a co-sedimentation assay. In this assay, c-actin can be co-sedimented due to its filamentous nature, whereas non-filamentous or non-interacting proteins remain in the supernatant. In the absence of c-actin, WT MyBP-C C0-C2 recombinant protein remained in the supernatant fraction. However, when cardiac actin was added to the assay, WT MyBP-C C0-C2 recombinant protein specifically bound and co-sedimented with c-actin as the recombinant protein was detected in the pellet. After a series of optimization experiments, we found that 2 μM of MyBP-C recombinant C0-C2 domains can specifically bind to 30 μM actin in a fully saturated manner (Figure 7A). 2 μM of each MyBP-C C0-C2 recombinant protein (WT and mutants) was incubated with c-actin at RT for 30 min and centrifuged for 1 hour at 14,000 g. The experiment was repeated with a different batch of recombinant proteins. The amounts of MyBP-C C0-C2 fragments in the supernatant fractions (unbound fractions) were analyzed by SDS-PAGE and quantified by Coomassie brilliant blue (Figure 7B) and densitometric analysis (Figure 7C). Following densitometric

analysis and % normalization of the binding of MyBP-C C0-C2 recombinant proteins to c-actin (Figure 7C), we found that except for V1, all the other variants (V2, V3, V4 and V5) displayed significantly reduced c-actin binding, with V4 and especially V5 showing the most dramatic reductions (~38 and 52% reduction of their c-actin relative binding affinities, respectively).

Discussion

HCM is a genetically heterogeneous autosomal dominant cardiac disease [4, 35], with many *c-MYBPC3* variants previously reported in HCM patients [1, 8]. Since HCM clinical presentation in patients is also heterogeneous, it is hypothesized that severity is correlated to underlying genetic mutations. Previous studies demonstrated that patients carrying specific mutations have been associated with earlier disease presentation, poorer prognosis, severe disease phenotype, higher prevalence of a family history and sudden cardiac death [32, 36, 37]. Furthermore, most of the childhood-onset disease mutations are missense (~76%), while ~60% of previously reported mutations in adults encode for MyBP-C truncations. This observation suggests that *c-MYBPC3* missense mutations causing HCM may be more severe than truncating mutations, explaining the earlier age of onset [38]. Some studies have established potential correlations in interpreting the phenotypic effect of these variants. However, the exact mechanism by which these variants affect MyBP-C physiological functions within the sarcomere leading to the different clinical phenotypes still remains unclear.

Our current study presents a new model of an *in vitro* functional genomics approach to investigate the effects of specific genotypes on MyBP-C biophysical and biochemical

characteristics that may explain HCM clinical severity. We selected five *c-MYBPC3* variants (Figure 1) that represented HCM heterogeneity with different pathogenicity classifications, as V3 and V5 (double mutant) were classified as the most pathogenic variants [11, 18-20]. Importantly, the double mutant V5 and the single mutant V3 exhibited the most severe myocardial hypertrophic phenotype (Table 1). Molecular modeling suggested critical structural consequences for these two variants (Figure 3). Furthermore, our biophysical analysis revealed that all variants lead to distinct protein conformations affecting the secondary structure content (Figure 4) and the thermodynamic stability (Figure 5) of the MyBP-C C0-C2 recombinant proteins. Consequently, distinct alterations of the MyBP-C C0-C2 fragments binding affinity to cardiac actin were observed when we investigated the protein interaction of these variants to cardiac actin (Figure 7).

Using different techniques of the zebrafish 'toolbox', we were able to recapitulate the different HCM phenotypes in the zebrafish model. All *c-MYBPC3* variants resulted in aberrant zebrafish cardiac morphology with altered ventricular size and function (Figure 2, supplemental material, 1). Our zebrafish experiments explored allele pathogenicity and captured specific cardiac phenotypes as effects that are variant-specific. The resultant zebrafish cardiac phenotype accurately resembled the human ventricular hypertrophic phenotype given that HCM patients exhibit increased myocardial wall thickness. Notably, V5 (E441K & E258K) and V3 (E258K) resulted in the most dramatic zebrafish cardiac impairment presenting with increased ventricular dimension in comparison to other variants. The V5 and V3 diastolic/systolic myocardial thickness was significantly increased and both variants exhibited significant contractile dysfunction with decreased heart rate in contrast to the other variants and wild-type MyBP-C. These results support the established class 5 pathogenicity of these two variants (Table 1).

Collectively, our zebrafish functional validation suggests an association of genotype to a disease phenotype; and confirmed the *in-silico* tools of pathogenicity classification of a specific genetic variant. Our findings support previous studies of other MyBP-C variants associated with a severe clinical phenotype [39]. Previous studies have demonstrated that each individual *c-MYBPC3* patient's phenotype varies with the position of the mutation and its cognate functional domain. It has been suggested that possessing multiple disease-causing sarcomere mutations may be associated with a greater risk for severe disease progression, including sudden cardiac death. This can be interpreted as double (or compound) variants exerting a gene dosage effect in HCM patients [9, 37, 40]. Recent reports using molecular modeling together with clinical and expression data revealed that the missense mutations in the C1-C2 of MyBP-C could be responsible for the severe symptoms studied in selected HCM patients [11, 13, 32]. Accordingly, our study particularly highlights the variants-induced secondary structural modifications in detail and reveal conformational rearrangements of the variants V3 and V5 (enhanced impact), which lead to severe effects on the motif region. As reported previously by many studies [31, 41], this motif is a key location for protein phosphorylation and for interaction with actin and/or myosin which serve to regulate the mechanism of muscular contractions. Therefore, the observed data from our modeling and CD-spectroscopy collectively suggest variation-induced secondary structural changes could be detrimental to function, explaining the abnormal phenotypes that we observed in our diseased models of zebrafish. Earlier molecular modeling suggested that V1 and V2 might increase the intra-molecular rigidity due to induced structural changes, resulting in minimal effect on the surface electrostatic properties that are key for binding with actin [13]. Contrastingly, V3 was predicted to significantly alter the structural properties leading to major change in C1 surface and malfunction of the protein [42]. Significantly, modeling of V5

conformational changes of C1-C2 domains predicted alterations of the binding of these domains to other MyBP-C domains and other sarcomeric proteins (actin and myosin), in particular by affecting the nearby motif region. These effects possibly explain the early onset and the severity of the observed HCM phenotype [11].

By using the zebrafish model to study the effects of these MyBP-C variants, our data indicate correlation of phenotypic variations to specific molecular mechanisms of altered protein characteristics and binding interactions with c-actin. The recombinant N-terminal, C0-C2 fragment, of V5 and V3 confirmed the model of altered secondary structural elements of the protein. As a result, V5 had only one unfolding transition step in the thermal denaturation curve compared to the other variants, which demonstrated two consecutive unfolding transitions. These observations highlight the fact that these missense variants result in altered protein conformations, which could potentially affect MyBP-C physiological functions within the sarcomere. MyBP-C is a multi-modular structural protein of 11 domains regulating sarcomere organization and contractility [1, 15, 43, 44]. It was previously shown that the N-terminal complex, C1-C2 of MyBP-C, regulates cardiac muscle contraction through actin interaction within the sarcomere [15, 28, 45, 46]. Our *in vitro* MyBP-C/cardiac actin co-sedimentation assays confirmed the negative effect of V2, V3, V4 and V5 mutations on the intermolecular interactions of MyBP-C with c-actin and more importantly highlighted the severe effect of the double mutation, V5. Accordingly, V5 relative binding affinity to c- actin was reduced almost 52% when compared to that of WT. In contrast, V1 variant did not exhibit any significant reduction on its relative binding affinity to c-actin suggesting alternative disease mechanisms rather than altered c-actin binding affinity. As recent studies have shown a significant overlap between the N-terminal of MyBP-C and actin as well as myosin S2 binding sites [47], further

analysis should be considered to study the impact of these variants on their interaction with myosin. Interestingly, despite the fact that we detected a significant reduction of V3 relative binding affinity to c-actin (~27%), earlier studies using the yeast two-hybrid system indicated that MyBP-C N-terminal E258K variant (V3) had reduced affinity to myosin heavy chain sub-fragment 2, providing a potential alternative mechanism underlying the HCM disease phenotype [48]. Our findings might begin to explain the contractile dysfunction resulting from the different *c-MYBPC3* variants as a result of their divergent biochemical and biophysical characteristics. Interestingly, the effect of the five mutations on cardiac phenotype in our experimental zebrafish model is consistent with previously reports on the patients' clinical severity.

Conclusion

Although MyBP-C protein has been extensively studied, the exact molecular mechanism(s) by which MyBP-C missense variants lead to severe cardiac disease remain elusive. This is largely due to the lack of a comprehensive understanding of the impact of these mutations on the protein molecular characteristics, as well as on its interactions with other sarcomeric components.

Our current study has clearly demonstrated that the zebrafish model is a very useful *in vivo* 'tool' to prognose and characterize the pathogenicity of MyBP-C missense mutations identified in patients with cardiac disease. It also provides further evidence for the important role of MyBP-C N-terminal C0-C2 domain on the vital interaction of this protein with actin within the sarcomere. However, taking into consideration that our observations are based on the *in vitro* biochemical and biophysical characterization of the isolated C0-C2 domains of MyBP-C protein and not of the full-length molecule, further *in vivo* studies are required to confirm and expand on our findings. We cannot exclude the possibility that the behavior of the full-length wild type

MyBP-C protein and its corresponding variants might be very different *in vivo*, necessitating further *in vivo* functional analysis, which will shed more light into the molecular mechanism(s) that mutations in *c-MYBPC3* gene lead to severe cardiac disease.

ACKNOWLEDGEMENTS

We thank Ms Rola Salem for her technical assistance with the protein expression and purification experiments.

DECLARATIONS OF INTEREST: The authors declare no financial interests.

FUNDING

M.N. was supported by internal CMED (QU) funding. A.T. was supported by the IKY scholarships programme through the action entitled "Reinforcement of Postdoctoral Researchers'', in the framework of the "Human Resources Development Program, Education and Lifelong Learning" of the National Strategic Reference Framework (NSRF) 2014-2020.

AUTHOR CONTRIBUTIONS

S.I.D., K.F. and M.N. devised the project strategy. S.I.D., K.F., B.S.G., E.T., G.N., F.A.L. and M.N. designed/analyzed the experiments, which were performed by S.I.D, A.T., A.S., B.L.C., and M.N. Molecular modeling was performed by N.K. Finally, S.I.D. and M.N. prepared the first manuscript draft, which was revised and approved by all authors.

References

1 Mohamed, I. A., Krishnamoorthy, N. T., Nasrallah, G. K. and Da'as, S. I. (2017) The Role of Cardiac Myosin Binding Protein C3 in Hypertrophic Cardiomyopathy-Progress and Novel Therapeutic Opportunities. *J. Cell. Physiol.* **232**, 1650-1659

2 Semsarian, C., Ingles, J., Maron, M. S. and Maron, B. J. (2015) New perspectives on the prevalence of hypertrophic cardiomyopathy. *J. Am. Coll. Cardiol.* **65**, 1249-1254

3 Varnava, A. M., Elliott, P. M., Mahon, N., Davies, M. J. and McKenna, W. J. (2001) Relation between myocyte disarray and outcome in hypertrophic cardiomyopathy. *Am. J. Cardiol.* **88**, 275-279
4 Marsiglia, J. D. C. and Pereira, A. C. (2014) Hypertrophic cardiomyopathy: how do mutations lead to disease? *Arq. Bras. Cardiol.* **102**, 295-304
5 Houston, B. A. and Stevens, G. R. (2015) Hypertrophic cardiomyopathy: a review. *Clin. Med. Insights Cardiol.* **8**, 53-65
6 Sen-Chowdhry, S., Jacoby, D., Moon, J. C. and McKenna, W. J. (2016) Update on hypertrophic cardiomyopathy and a guide to the guidelines. *Nat. Rev. Cardiol.* **13**, 651-675
7 Olivotto, I., d'Amati, G., Basso, C., Van Rossum, A., Patten, M., Emdin, M., Pinto, Y., Tomberli, B., Camici, P. G. and Michels, M. (2015) Defining phenotypes and disease progression in sarcomeric cardiomyopathies: contemporary role of clinical investigations. *Cardiovasc. Res.* **105**, 409-423
8 Carrier, L., Mearini, G., Stathopoulou, K. and Cuello, F. (2015) Cardiac myosin-binding protein C (MYBPC3) in cardiac pathophysiology. *Gene* **573**, 188-197
9 Maron, B. J., Maron, M. S. and Semsarian, C. (2012) Double or compound sarcomere mutations in hypertrophic cardiomyopathy: a potential link to sudden death in the absence of conventional risk factors. *Heart Rhythm* **9**, 57-63
10 Fourey, D., Almansoori, G., Care, M., Rakowski, H. and Chan, R. H. (2015) Double or Compound Sarcomere Mutations in Hypertrophic Cardiomyopathy is Not Associated With Worsened Outcomes: A Single Center Cohort Study. *Circulation* **132,** 18559
11 Gajendrarao, P., Krishnamoorthy, N., Selvaraj, S., Girolami, F., Cecchi, F., Olivotto, I. and Yacoub, M. (2015) An investigation of the molecular mechanism of double cMyBP-C mutation in a patient with end-stage hypertrophic cardiomyopathy. *J. Cardiovasc. Transl. Res.* **8**, 232-243
12 Liu, X., Jiang, T., Piao, C., Li, X., Guo, J., Zheng, S., Zhang, X., Cai, T. and Du, J. (2015) Screening mutations of MYBPC3 in 114 unrelated patients with hypertrophic cardiomyopathy by targeted capture and next-generation sequencing. *Sci. Rep.* **5,** 11411
13 Gajendrarao, P., Krishnamoorthy, N., Kassem, H. S., Moharem-Elgamal, S., Cecchi, F., Olivotto, I. and Yacoub, M. H. (2013) Molecular modeling of disease causing mutations in domain C1 of cMyBP-C. *PloS one* **8**, e59206
14 Schlossarek, S., Englmann, D. R., Sultan, K. R., Sauer, M., Eschenhagen, T. and Carrier, L. (2012) Defective proteolytic systems in Mybpc3-targeted mice with cardiac hypertrophy. *Basic Res. Cardiol.* **107**, 235
15 Sadayappan, S. and de Tombe, P. P. (2012) Cardiac myosin binding protein-C: redefining its structure and function. *Biophys. Rev.* **4**, 93-106
16 Rybakova, I. N., Greaser, M. L. and Moss, R. L. (2011) Myosin binding protein c interaction with actin characterization and mapping of the binding site. *J. Biol. Chem.* **286**, 2008-2016
17 Stanczyk, P. J., Seidel, M., White, J., Viero, C., George, C. H., Zissimopoulos, S. and Lai, F. A. (2018) Association of cardiac myosin-binding protein-C with the ryanodine receptor channel - putative retrograde regulation? *J. Cell Sci.* **131,** 210443
18 Jaafar, N., Gómez, J., Kammoun, I., Zairi, I., Ben Amara, W., Kachboura, S., Kraiem, S., Hammami, M., Iglesias, S., Alonso, B. and Coto, E. (2016) Spectrum of Mutations in Hypertrophic Cardiomyopathy Genes Among Tunisian Patients. *Genet. Test Mol. Biomarkers* **20**, 674-679
19 Rodríguez-García, M. I., Monserrat, L., Ortiz, M., Fernández, X., Cazón, L., Núñez, L., Barriales-Villa, R., Maneiro, E., Veira, E. and Castro-Beiras, A. (2010) Screening mutations in myosin binding protein C3 gene in a cohort of patients with Hypertrophic Cardiomyopathy. *BMC Med. Genet.* **11**, 67
20 Marsiglia, J. D. C., Batitucci, M. d. C. P., Paula, F. d., Barbirato, C., Arteaga, E. and Araújo, A. Q. d. (2010) Study of mutations causing hypertrophic cardiomyopathy in a group of patients from Espirito Santo, Brazil. *Arq. Bras. Cardiol.* **94**, 10-17

21 Kassem, H. S., Azer, R. S., Ayad, M. S., Moharem-Elgamal, S., Magdy, G., Elguindy, A., Cecchi, F., Olivotto, I. and Yacoub, M. H. (2013) Early results of sarcomeric gene screening from the Egyptian National BA-HCM Program. *J. Cardiovasc. Transl. Res.* **6**, 65-80
22 Reed, B. and Jennings, M. (2011) Guidance on the housing and care of zebrafish *Danio rerio*. *Southwater: Royal Society for the Prevention of Cruelty to Animals*
23 Chen, Y.-H., Pai, C.-W., Huang, S.-W., Chang, S.-N., Lin, L.-Y., Chiang, F.-T., Lin, J.-L., Hwang, J.-J. and Tsai, C.-T. (2013) Inactivation of Myosin binding protein C homolog in zebrafish as a model for human cardiac hypertrophy and diastolic dysfunction. *J. Am. Heart Assoc.* **2**, e000231
24 Nomikos, M., Thanassoulas, A., Beck, K., Vassilakopoulou, V., Hu, H., Calver, B. L., Theodoridou, M., Kashir, J., Blayney, L., Livaniou, E., Rizkallah, P., Nounesis, G. and Lai, F. A. (2014) Altered RyR2 regulation by the calmodulin F90L mutation associated with idiopathic ventricular fibrillation and early sudden cardiac death. *FEBS Lett.* **588**, 2898-2902
25 Vassilakopoulou, V., Calver, B. L., Thanassoulas, A., Beck, K., Hu, H., Buntwal, L., Smith, A., Theodoridou, M., Kashir, J., Blayney, L., Livaniou, E., Nounesis, G., Lai, F. A. and Nomikos, M. (2015) Distinctive malfunctions of calmodulin mutations associated with heart RyR2-mediated arrhythmic disease. *Biochim. Biophys. Acta* **1850**, 2168-2176
26 Nomikos, M., Blayney, L. M., Larman, M. G., Campbell, K., Rossbach, A., Saunders, C. M., Swann, K. and Lai, F. A. (2005) Role of phospholipase C-ζ domains in Ca2+-dependent phosphatidylinositol 4, 5-bisphosphate hydrolysis and cytoplasmic Ca2+ oscillations. *J. Biol. Chem.* **280**, 31011-31018
27 Fersht, A. (1999) Structure and mechanism in protein science : a guide to enzyme catalysis and protein folding. W.H. Freeman, New York
28 Shaffer, J. F., Kensler, R. W. and Harris, S. P. (2009) The myosin-binding protein C motif binds to F-actin in a phosphorylation-sensitive manner. *J. Biol. Chem.* **284**, 12318-12327
29 Poon, K. L. and Brand, T. (2013) The zebrafish model system in cardiovascular research: A tiny fish with mighty prospects. *Glob. Cardiol. Sci. Pract.* **4**, 9-28
30 Olivotto, I., Maron, M. S., Autore, C., Lesser, J. R., Rega, L., Casolo, G., De Santis, M., Quarta, G., Nistri, S. and Cecchi, F. (2008) Assessment and significance of left ventricular mass by cardiovascular magnetic resonance in hypertrophic cardiomyopathy. *J. Am. Coll. Cardiol.* **52**, 559-566
31 Luther, P. K. and Vydyanath, A. (2011) Myosin binding protein-C: an essential protein in skeletal and cardiac muscle. *J. Muscle Res. Cell Motil.* **31**, 303-305
32 Krishnamoorthy, N., Gajendrarao, P., Olivotto, I. and Yacoub, M. (2017) Impact of disease-causing mutations on inter-domain interactions in cMyBP-C: a steered molecular dynamics study. *J. Biomol. Struct. Dyn.* **35**, 1916-1922
33 Brown, L. J., Singh, L., Sale, K. L., Yu, B., Trent, R., Fajer, P. G. and Hambly, B. D. (2002) Functional and spectroscopic studies of a familial hypertrophic cardiomyopathy mutation in Motif X of cardiac myosin binding protein-C. *Eur. Biophys. J.* **31**, 400-408
34 Michalek, A. J., Howarth, J. W., Gulick, J., Previs, M. J., Robbins, J., Rosevear, P. R. and Warshaw, D. M. (2013) Phosphorylation modulates the mechanical stability of the cardiac myosin-binding protein C motif. *Biophys. J.* **104**, 442-452
35 Schlossarek, S., Mearini, G. and Carrier, L. (2011) Cardiac myosin-binding protein C in hypertrophic cardiomyopathy: mechanisms and therapeutic opportunities. *J. Mol. Cell. Cardiol.* **50**, 613-620
36 Rafael, J. F., Cruz Filho, F. E. d. S., Carvalho, A. C. C. d., Gottlieb, I., Cazelli, J. G., Siciliano, A. P. and Dias, G. M. (2017) Myosin-binding Protein C Compound Heterozygous Variant Effect on the Phenotypic Expression of Hypertrophic Cardiomyopathy. *Arq. Bras. Cardiol.* **108**, 354-360
37 Lopes, L. R., Rahman, M. S. and Elliott, P. M. (2013) A systematic review and meta-analysis of genotype–phenotype associations in patients with hypertrophic cardiomyopathy caused by sarcomeric protein mutations. *Heart* **99**, 1800-1811

38 Teekakirikul, P., Kelly, M. A., Rehm, H. L., Lakdawala, N. K. and Funke, B. H. Inherited Cardiomyopathies. *J. Mol. Diagn.* **15**, 158-170
39 Hodatsu, A., Konno, T., Hayashi, K., Funada, A., Fujita, T., Nagata, Y., Fujino, N., Kawashiri, M.-a. and Yamagishi, M. (2014) Compound heterozygosity deteriorates phenotypes of hypertrophic cardiomyopathy with founder MYBPC3 mutation: evidence from patients and zebrafish models. *J. Physiol. Heart Circ. Physiol.* **307**, 1594-1604
40 Lopes, L. R., Zekavati, A., Syrris, P., Hubank, M., Giambartolomei, C., Dalageorgou, C., Jenkins, S., McKenna, W., Plagnol, V. and Elliott, P. M. (2013) Genetic complexity in hypertrophic cardiomyopathy revealed by high-throughput sequencing. *J. Med. Genet.* **50**, 228-239
41 Previs, M. J., Prosser, B. L., Mun, J. Y., Previs, S. B., Gulick, J., Lee, K., Robbins, J., Craig, R., Lederer, W. and Warshaw, D. M. (2015) Myosin-binding protein C corrects an intrinsic inhomogeneity in cardiac excitation-contraction coupling. *Sci. Adv.* **1**, e1400205
42 Da'as, S. I., Yu, J., Butcher, J. T., Krishnamoorthy, N., Al Suwaidi, J. A. S., Kassem, H., Al Shafai, K. N., Al-Hashemi, M. A., Shuayb, L. and Brand, T. (2014) Different human mutations in the myosin binding protein C3 (MYBPC3) produce specific cardiac phenotypes in the zebrafish. *Circulation* **130**, 17545
43 Schlossarek, S. and Carrier, L. (2011) The ubiquitin–proteasome system in cardiomyopathies. *Curr. Opin. Cardiol.* **26**, 190-195
44 Pfuhl, M. and Gautel, M. (2012) Structure, interactions and function of the N-terminus of cardiac myosin binding protein C (MyBP-C): who does what, with what, and to whom? *J. Muscle Res. Cell Motil.* **33**, 83-94
45 Kensler, R. W., Shaffer, J. F. and Harris, S. P. (2011) Binding of the N-terminal fragment C0–C2 of cardiac MyBP-C to cardiac F-actin. *J. Struct. Biol.* **174**, 44-51
46 Belknap, B., Harris, S. P. and White, H. D. (2014) Modulation of thin filament activation of myosin ATP hydrolysis by N-terminal domains of cardiac myosin binding protein-C. *Biochemistry* **53**, 6717-6724
47 Bhuiyan, M. S., Gulick, J., Osinska, H., Gupta, M. and Robbins, J. (2012) Determination of the critical residues responsible for cardiac myosin binding protein C's interactions. *J. Mol. Cell. Cardiol.* **53**, 838-847
48 De Lange, W. J., Grimes, A. C., Hegge, L. F., Spring, A. M., Brost, T. M. and Ralphe, J. C. (2013) E258K HCM-causing mutation in cardiac MyBP-C reduces contractile force and accelerates twitch kinetics by disrupting the cMyBP-C and myosin S2 interaction. *J. Gen. Physiol.* **142**, 241-255

Table Legends

Table 1. Hypertrophic cardiomyopathy associated c-*MYBPC3* missense mutations location, classification and clinical characteristics. a: variant (V) reported at ClinVar database (https://www.ncbi.nlm.nih.gov/clinvar/), b: V5, patient carrying double mutation of V3 and V4, c: reference sequence NM_000256.3, d: protein sequence NP_000247.2, e: frequency allele reported at ExAC = Exome Aggregation Consortium (http://exac.broadinstitute.org), N/R (not reported), f: age of disease onset, g: cardiac septum thickness, h: interpretation of sequence

variants pathogenicity based on American College of Medical Genetics and Genomics (ACMG) guidance.

Table 2. Secondary structure elements for all recombinant proteins at 25°C.

Table 3. Thermodynamic parameters calculated from chemical denaturation experiments for WT and MyBP-C variants.

Figure Legends

Figure 1. **Location of hypertrophic cardiomyopathy associated mutations.** Schematic illustration showing **A.** Cardiac myosin binding protein C3 (*c-MYBPC3*), showing the location of hypertrophic cardiomyopathy variants in Human Genetics Variants Society (HGVS) format, The c-*MYBPC3* is composed of 35 exons, where these variants are located within exon 5, 6 and 13. **B.** MyBP-C protein consists of 11 domains (C0-C10); 8 immunoglobulin-like domains (IgC2-like) and 3 fibronectin type III-like (FN3) domains with N-terminal Proline-Alanine rich linker sequence and the regulatory Motif that includes the phosphorylation sites indicated by asterisks. All variants in this study are within the C1-C2 domains.

Figure 2. Expression of *c-MYBPC3* variants in the zebrafish model recapitulated the human HCM phenotype. A. Zebrafish injected with human *c-MYBPC3* synthetic RNA of wild type and the five variants at one cell stage. At 72 hours post fertilization, larvae were mounted posteriorly to image ventricle chamber of the heart (black box). **B.** Representative images of aberrant heart morphology of the five expressed variants in comparison to control group. **C.** Cardiac functional analysis of variants expressed in zebrafish, the measurement of ventricular diastolic myocardial thickness for V5 (double mutation E441K & E258K) and V3 (E258K) were the most significantly increased mean followed by V1 (R177H), V4 (E441K) and V2 (A216T) in comparison to WT. **D.** Ventricular systolic myocardial thickness measurement for V5 were the most significantly increased mean at 14.6 µm followed by V3, V1, V4 and V2 in comparison to WT. **E.** Heart contractile measurement showed that both V5 and V3 significantly impacted the

average heart rate in injected zebrafish demonstrated by the significant reduced heart rate mean measured by beats per minute (bpm) compared to WT. While, V1, V2 and V4 heart rates were still less than the control zebrafish. Cardiac function analyses were represented in Box – Whisker plots and analysis using one-way ANOVA multiple comparisons test. Values were expressed as means ± SE and *p* values of < 0.05 were considered statistically significant, a value of **p<0.01, ***p<0.001 and ***p<0.0001.

Figure 3. Molecular model of the structural analysis of V5 and V3. A. MyBP-C WT 3D structure. **B.** Structural comparison of WT vs V3. **C.** Structural comparison of WT vs V5. Both V5 and V3 deviated structurally and rearranged differently from the WT illustrated mainly in elements rearrangement at the motif region. **D.** Root mean square deviation (RMSD) calculation of the representative structures from molecular dynamics simulations illustrated that V3 conformational deviation appeared to be flexible, while V5 showed more rigid behavior. **E.** Secondary structural change analysis of intra-molecular consequences. V3 model illustrated reduced β-sheets content and increased coils content compared to WT, however, V5 showed inverse behavior. This analysis correlated with the deviation analysis and explained the flexibility of V3 as there is increase of coils and for the rigidity of V5 due to the reduction of coils and increase of β-sheets contents.

Figure 4. Expression, purification and intein cleavage of C0-C2 (MyBP-C) recombinant protein fragment. A. Schematic diagram showing the C0-C2 domains fragment and its proposed interaction with cardiac actin. **B.** Analysis of recombinant expression and purification of C0-C2 fragment protein of WT, V1, V2, V3, V4 and V5 (V3+V4) of equivalent volumes at 12% SDS-PAGE by Coomassie staining and western blot with a polyclonal MyBP-C antibody (1:1000 dilution). **C.** MyBP-C circular dichroism (CD) spectra measurements at 25°C. All variants disrupted the structure of the protein fragment leading to conformations with altered secondary structure characteristics impacting the fragment elements; predominantly the β-sheet, random coil content and helical content when compared to WT. However, V5 (double mutation) resulted in the most altered secondary structure in comparison to WT. (WT:black, V1:red, V2:green, V3:blue, V4:cyan and V5:pink).

Figure 5. Thermal denaturation profile of MyBP-C recombinant protein fragments measured as normalized CD signal at 208 nm. The thermal denaturation curve of WT, V1, V2, V3 and V4 reveals the presence of two consecutive unfolding transitions at which the first thermal transition occurs in the temperature range 50°C - 65°C and the second in the temperature range 65°C - 90°C. while, in contrast, the melting profile of V5 indicated only the first unfolding transition at 50°C - 65°C, indicating that no further aggregation occurs after ~60°C for this fragment.

Figure 6. Chemical denaturation trace of MyBP-C recombinant protein fragments. Changes in the weighted average emission wavelength (excitation 295 nm) of MyBP-C WT and the different variants were measured in solution upon titration with increasing amounts of the chemical denaturant guanidine hydrochloride (GuHCl). All MyBP-C fragments had displayed reversible transition presented by Sigmoidal two-state denaturation curves for the fraction of unfolding. Calculated Gibbs free energy change (ΔG) of the unfolding process illustrated increased stability for all variants except V5 in comparison to WT.

Figure 7. Co-sedimentation binding assays of MyBP-C C0-C2 recombinant proteins and cardiac actin (c-actin). MyBP-C C0-C2 recombinant proteins (2 μM) were incubated with c-actin at RT for 30 min and spun for 1 hour at 14,000 g. The amount of MyBP-C C0-C2 proteins in supernatant (unbound fraction) was analyzed by SDS-PAGE and quantified by Coomassie brilliant blue and densitometric analysis. (A) Optimization experiments using 2 μM of MyBP-C C0-C2 WT and 20 or 30 μM c-actin showing that saturated binding is achieved with 30 μM c-actin. (B) Representative SDS-PAGE gel and Coomassie brilliant blue staining following MyBP-C C0-C2 mutant protein-c-actin co-sedimentation assays showing the amounts of MyBP-C C0-C2 mutant proteins in supernatant fractions (unbound fraction) pre (-) and post (+) co-sedimentation with 30 μM c-actin. (C) Densitometric analysis and % normalization of the binding of MyBP-C C0-C2 recombinant proteins to 30 μM c-actin. Significant effects (asterisks) were calculated by comparison to the binding of WT MyBP-C C0-C2 using an unpaired Student's t-test. n = 2 ± S.E.M., *$p<0.05$ and **$p<0.01$, (GraphPad Prism 7).

Tables

Table 1

Variant [a] (V)	c-MYBPC3 [c]	MyBP-C [d]	ExAC allele frequency [e]	MyBP-C Domain	Years [f]	Thickness [g] (mm)	HCM patients clinical symptoms	Classification of Pathogenicity [h]	Reference
V1	c.530G>A	p.Arg177His	0.0009493	C1 (Ig-like C2-type 1)	56	15	Chest pain	Unlikely to be pathogenic	(Jaafar, Gómez et al. 2016)
V2	c.646G>A	p.Ala216Thr	0.000365	C1 (Ig-like C2-type 1)	34	N/R	Sub-aortic occlusion	Class 3- Unknown pathogenicity	(Rodríguez-García, Monserrat et al. 2010)
V3	c.772G>A	p.Glu258Lys	3.9E-05	M-motif (phosphorylation site)	49	15	chest pain and palpitation, chest pain and dyspnea	Class 5- Certainly pathogenic	(Jaafar, Gómez et al. 2016)
V4	c.1321G>A	p.Glu441Lys	0.000162	C2 (Ig-like C2-type 2)	45	23.2	no syncope, complaint about angina at exertion, but no ventricular tachycardia	Class 3- Unknown pathogenicity	(Marsiglia, Batitucci et al. 2010)
V5 [b] (V3 + V4)	c.772G>A +c.1321G>A	p.(Glu258Lys + Glu441Lys)	-	M motif and C2 (Ig-like C2-type 2)	21	22	dyspnea, progressive heart failure with repeated hospitalizations then patient died at age 42	Class 5- Certainly pathogenic	(Gajendrarao, Krishnamoorthy et al. 2015)

Table 2

Protein	α-Helix	β-Sheet		β-Turn	Random Coil
		Antiparallel	Parallel		
WT	20.7%	11.3%	13.6%	18.9%	40.2%
V1	26.8%	21.2%	8.9%	19.1%	28.1%
V2	26.4%	11.1%	10.6%	18.4%	36.4%
V3	26.8%	14.4%	9.9%	18.2%	33.7%
V4	26.0%	10.6%	10.7%	18.4%	38.5%
V5	26.8%	21.2%	8.9%	19.1%	28.5%

Table 3

Protein	m (kcal mol^{-1} M^{-1})	$D^{50\%}$ (M)	ΔG_{DN} (kcal mol^{-1})
WT	2.07 ± 0.15	1.67 ± 0.05	3.46 ± 0.27
V1	2.45 ± 0.19	1.66 ± 0.05	4.07 ± 0.34
V2	2.25 ± 0.15	1.77 ± 0.03	3.98 ± 0.27
V3	2.90 ± 0.21	1.69 ± 0.03	4.90 ± 0.37
V4	2.83 ± 0.20	1.76 ± 0.03	4.98 ± 0.36
V5	2.03 ± 0.16	1.56 ± 0.03	3.17 ± 0.26

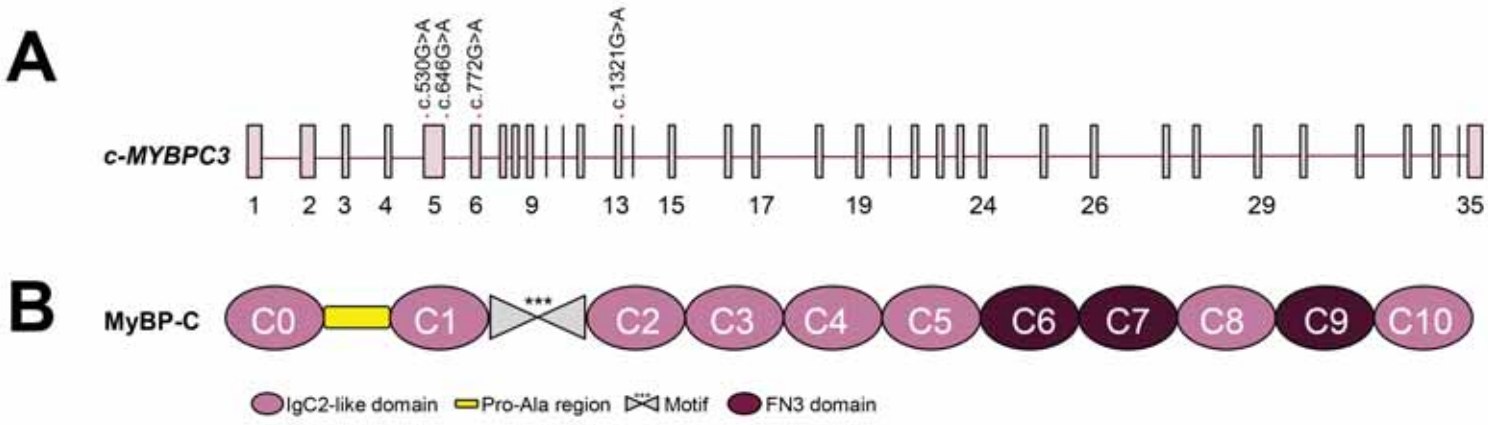
A
c.530G>A
c.646G>A
c.772G>A
c.1321G>A
c-MYBPC3
1 2 3 4 5 6 9 13 15 17 19 24 26 29 35
B
MyBP-C
C0 C1 *** C2 C3 C4 C5 C6 C7 C8 C9 C10
IgC2-like domain
Pro-Ala region
Motif
FN3 domain

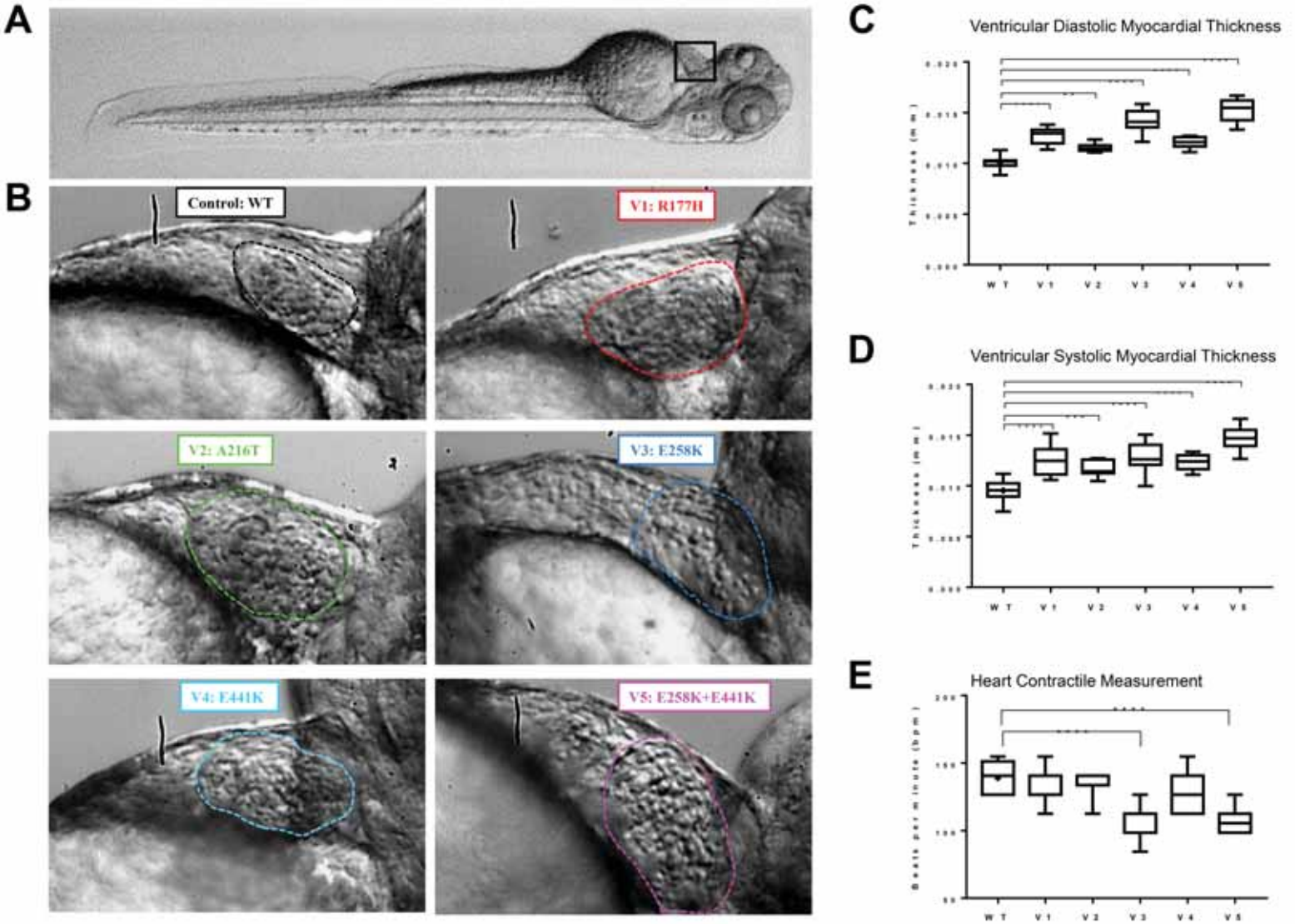
A
B
Control: WT
V1: R177H
V2: A216T
V3: E258K
V4: E441K
V5: E258K+E441K
C
Ventricular Diastolic Myocardial Thickness
D
Ventricular Systolic Myocardial Thickness
E
Heart Contractile Measurement

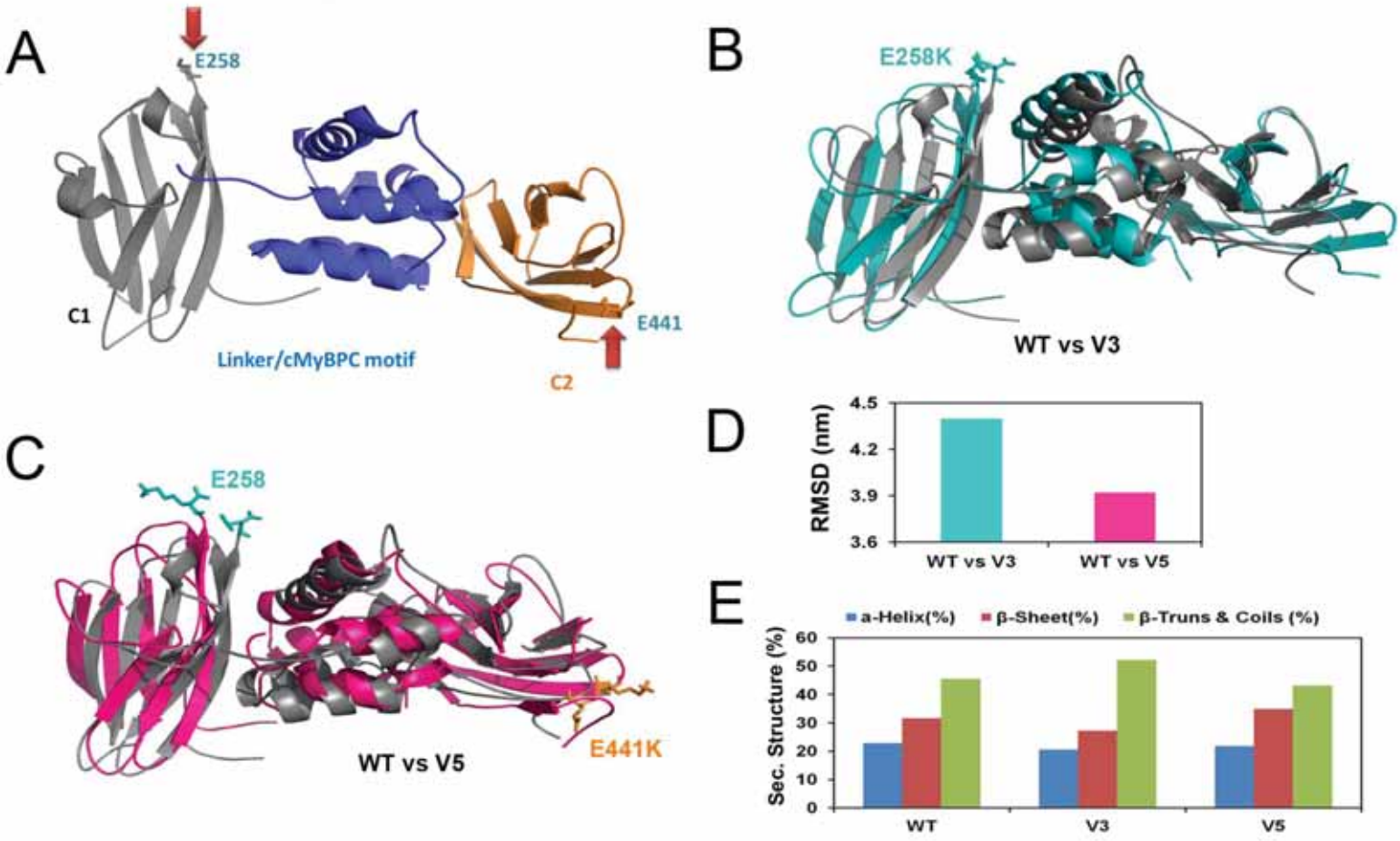
A
E258
C1
Linker/cMyBPC motif
E441
C2
B
E258K
WT vs V3
C
E258
E441K
WT vs V5
D
RMSD (nm)
4.5
4.2
3.9
3.6
WT vs V3
WT vs V5
E
a-Helix(%)
β-Sheet(%)
β-Truns & Coils (%)
Sec. Structure (%)
60
50
40
30
20
10
0
WT
V3
V5

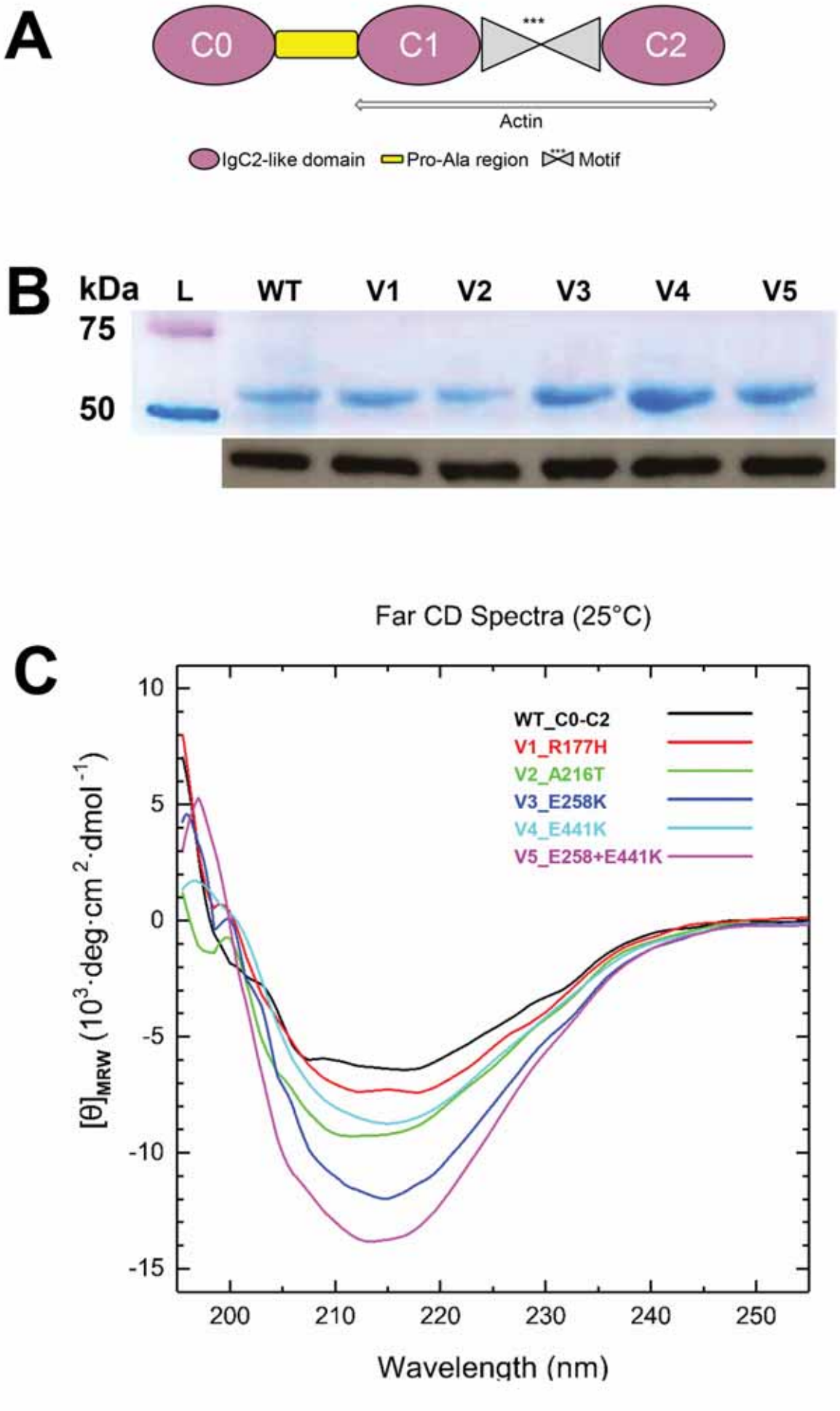
A
C0
C1
C2
***
Actin
IgC2-like domain
Pro-Ala region
Motif
B
kDa
L
WT
V1
V2
V3
V4
V5
75
50
C
Far CD Spectra (25°C)
WT_C0-C2
V1_R177H
V2_A216T
V3_E258K
V4_E441K
V5_E258+E441K
[θ]MRW (10^3·deg·cm^2·dmol^-1)
10
5
0
-5
-10
-15
200
210
220
230
240
250
Wavelength (nm)

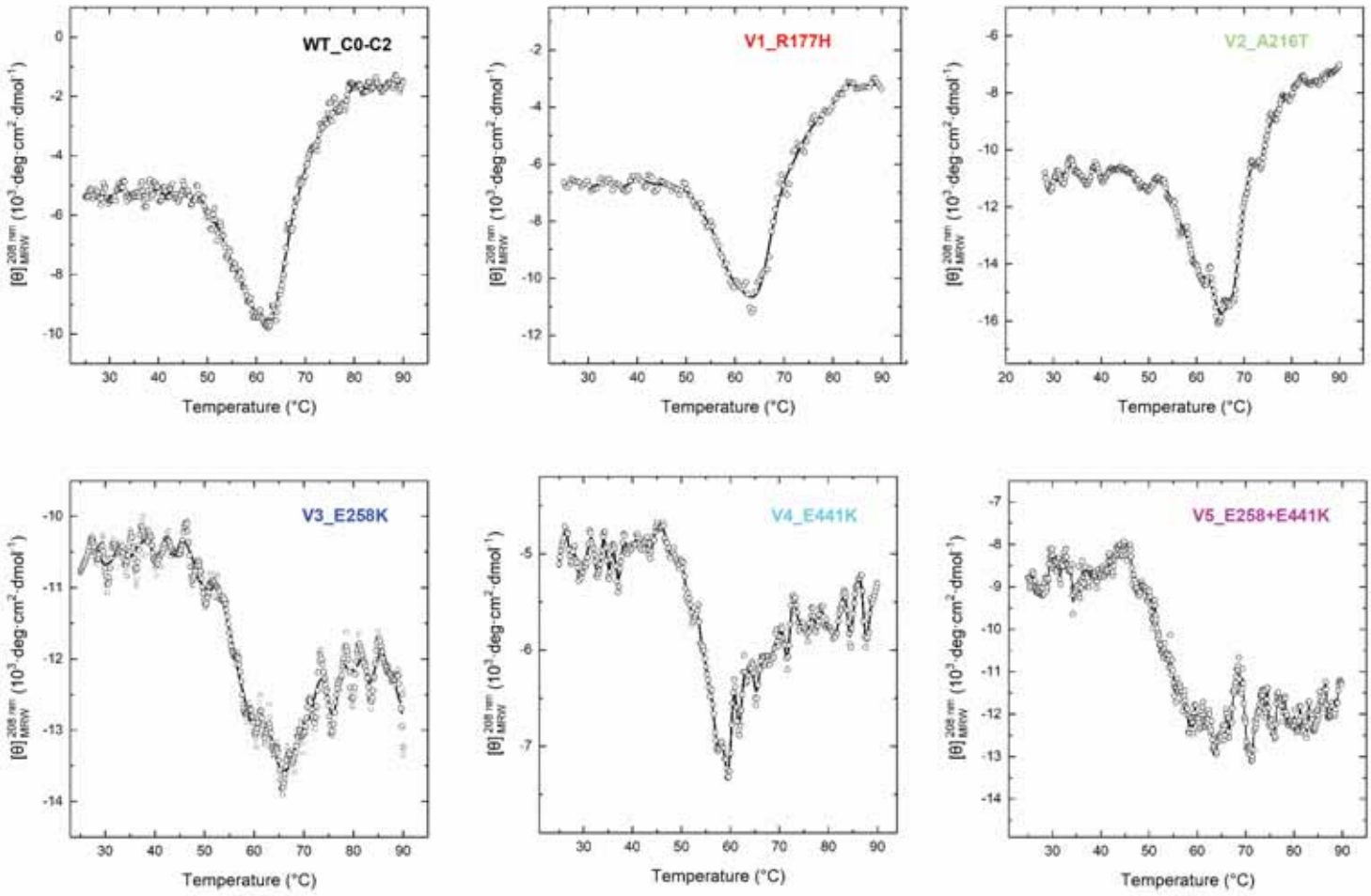
WT_C0-C2
V1_R177H
V2_A216T
V3_E258K
V4_E441K
V5_E258+E441K
Temperature (°C)
[θ]208 nm MRW (10³·deg·cm²·dmol⁻¹)

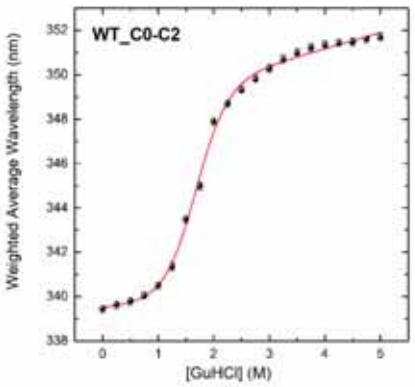
WT_C0-C2
Weighted Average Wavelength (nm)
[GuHCl] (M)

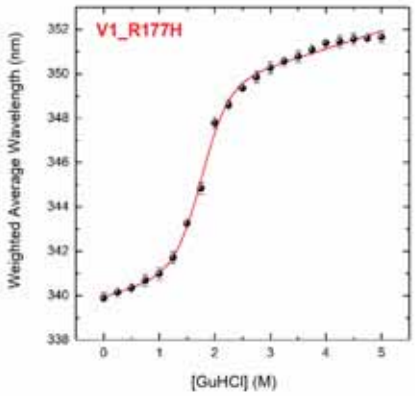
V1_R177H
Weighted Average Wavelength (nm)
[GuHCl] (M)

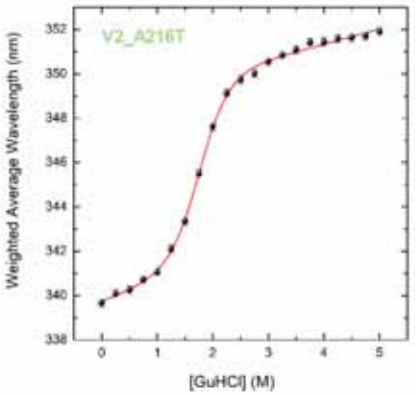
V2_A216T
Weighted Average Wavelength (nm)
[GuHCl] (M)

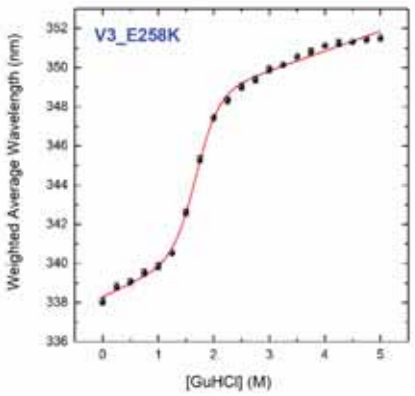
V3_E258K
Weighted Average Wavelength (nm)
[GuHCl] (M)

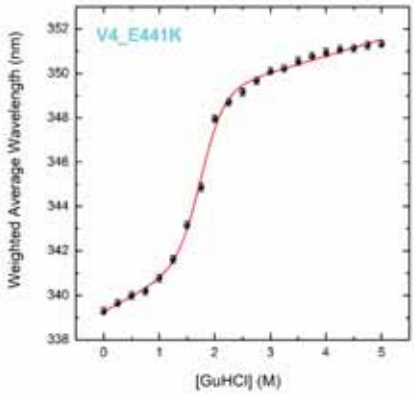
V4_E441K
Weighted Average Wavelength (nm)
[GuHCl] (M)

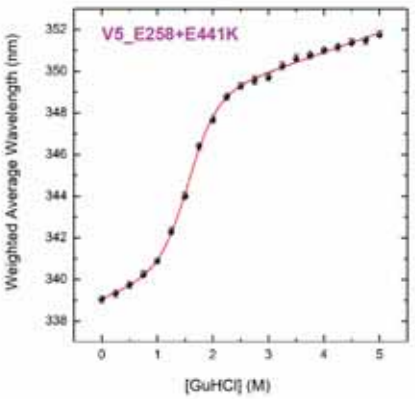
V5_E258+E441K
Weighted Average Wavelength (nm)
[GuHCl] (M)

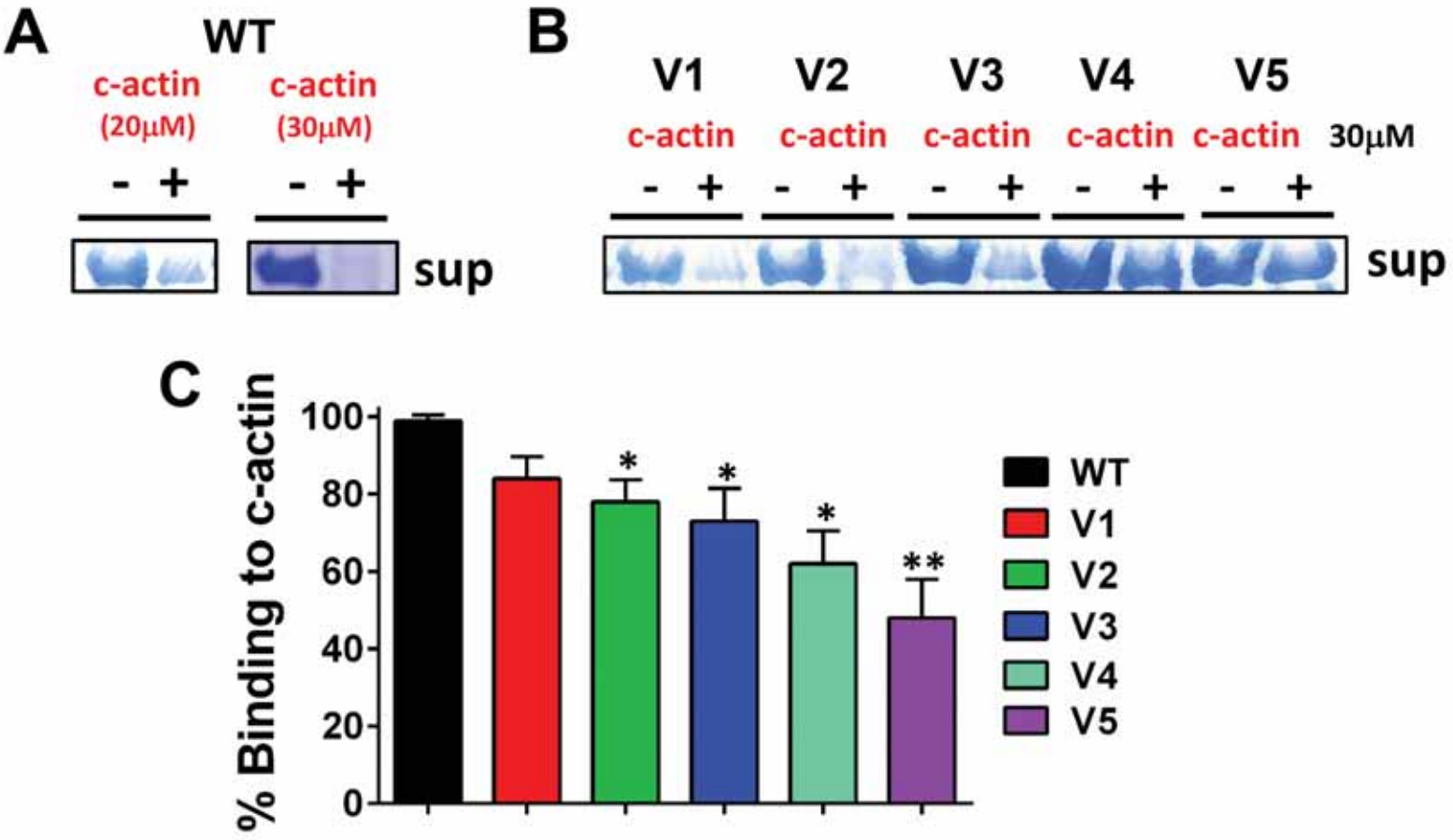
A
WT
c-actin
(20μM)
c-actin
(30μM)
- + - +
sup
B
V1
V2
V3
V4
V5
c-actin
c-actin
c-actin
c-actin
c-actin
30μM
- + - + - + - + - +
sup
C
% Binding to c-actin
100
80
60
40
20
0
*
*
*
**
WT
V1
V2
V3
V4
V5

Supplemental Material

Tables

Temperature (°C)	α-Helix	β-Sheet		β-Turn	Random Coil
		Antiparallel	Parallel		
25	20.7%	11.3%	13.6%	18.9%	40.2%
65	25.6%	9.9%	11.7%	18.0%	38.1%
90	11.1%	11.1%	12.6%	19.4%	50.4%

Table 1. Secondary structure elements for WT MyBP-C fragment at various temperatures.

Temperature (°C)	α-Helix	β-Sheet		β-Turn	Random Coil
		Antiparallel	Parallel		
25	26.8%	21.2%	8.9%	19.1%	28.1%
65	26.2%	10.9%	10.8%	18.2%	37.4%
90	12.1%	11.6%	12.8%	19.4%	49.1%

Table 2. Secondary structure elements for V1 MyBP-C fragment at various temperatures.

Temperature (°C)	α-Helix	β-Sheet		β-Turn	Random Coil
		Antiparallel	Parallel		
25	26.4%	11.1%	10.6%	18.4%	36.4%
65	28.7%	12.7%	9.5%	17.8%	32.9%
90	17.9%	11.2%	13.7%	19.2%	45.3%

Table 3. Secondary structure elements for V2 MyBP-C fragment at various temperatures.

Temperature (°C)	α-Helix	β-Sheet		β-Turn	Random Coil
		Antiparallel	Parallel		
25	26.8%	14.4%	9.9%	18.2%	33.7%
65	25.9%	17.4%	9.4%	18.8%	29.9%
90	28.6%	14.8%	9.7%	18.2%	27.9%

Table 4. Secondary structure elements for V3 MyBP-C fragment at various temperatures.

Temperature (°C)	α-Helix	β-Sheet		β-Turn	Random Coil
		Antiparallel	Parallel		
25	26.0%	10.6%	10.7%	18.4%	38.5%
65	26.3%	11.1%	10.6%	18.3%	36.4%
90	25.7%	9.9%	11.7%	18.1%	39.5%

Table 5. Secondary structure elements for V4 MyBP-C fragment at various temperatures.

Temperature (°C)	α-Helix	β-Sheet		β-Turn	Random Coil
		Antiparallel	Parallel		
25	26.8%	21.2%	8.9%	19.1%	28.5%
65	30.4%	20.1%	7.6%	19.1%	26.4%
90	27.9%	19.9%	8.6%	19.6%	27.6%

Table 6. Secondary structure elements for V5 MyBP-C fragment at various temperatures.